*Articles*

# Two-Dimensional COSY and Two-Dimensional NOE Spectroscopy of $d(AC)_4 \cdot d(GT)_4$: Extraction of Structural Constraints†

Miriam Gochin, Gerald Zon,‡ and Thomas L. James*

*Departments of Pharmaceutical Chemistry and Radiology, University of California, San Francisco, California 94143*

*Received March 8, 1990; Revised Manuscript Received June 7, 1990*

ABSTRACT: Pure absorption phase, proton two-dimensional nuclear Overhauser effect (2D NOE) and double-quantum-filtered COSY (DQF-COSY) spectra were recorded for $d(AC)_4 \cdot d(GT)_4$. A full proton resonance assignment was made, except for the 5′ and 5″ protons. A new semiautomatic method for improved quantitation of 2D NOE peak intensities was developed, and its limitations and usefulness were examined. With this new method, 2D NOE intensity sets at several mixing times were obtained. Simulations of the 1′2′, 1′2″, and 2′3′ DQF-COSY cross-peaks were compared with experimental data, establishing an alternating sugar pucker for the alternating purine–pyrimidine sequence. Scalar coupling constants for the sugar ring protons, derived from the fitting of the simulated spectra, are reported. Complete relaxation matrix analysis of the 2D NOE spectrum verified this alternating structure for all NOE interactions between nonexchangeable protons. Both the DQF-COSY and the 2D NOE results qualitatively indicate that the structure of $d(AC)_4 \cdot d(GT)_4$ resembles wrinkled D-DNA in aqueous solution.

With the rapid advancement of two-dimensional NMR techniques in the last several years has come a spate of solution studies on DNA oligomers and proteins (Wüthrich, 1986). Coupled with this is the development of an array of computationally intensive methods for analyzing NMR data, namely, distance geometry (Havel et al., 1983), complete relaxation matrix analysis (Borgias et al., 1987, 1989), iterative relaxation matrix analysis (Borgias et al., 1988; Boelens et al., 1988; Borgias & James, 1990), COSY cross-peak simulation (Widmer & Wüthrich, 1986), and molecular mechanics and dynamics (Singh et al., 1986). The aim of the current study is to employ several of these analytical methods for study of the DNA octamer $d(AC)_4 \cdot d(GT)_4$. There is interest in understanding the structural features of alternating purine–pyrimidine duplexes, but we also have the intention of defining the limits of structural precision currently possible from NMR data. A particular question that will be addressed is whether NMR is capable of distinguishing between a time-averaged single conformer state and a multiconformer state. The study is divided into two consecutive papers. This first paper describes details of the experiment and a qualitative and semiquantitative analysis of the NMR data. It compares results obtained by COSY and 2D NOE spectroscopy on the same oligomer, a feature not described in the literature. The following paper entails a detailed molecular dynamics simulation study using the NMR data as constraints.

$d(AC)_4 \cdot d(GT)_4$ is an important oligomer in the general study of sequence-dependent structural effects. Observation of nonstandard structure (i.e., not standard A-DNA or B-DNA) for polynucleotides with alternating purine–pyrimidine sequences was originally made from fiber diffraction studies (Arnott et al., 1983). Poly[d(GC)]·poly[d(GC)] was observed to have a wrinkled B (wB) structure and poly[d(AT)]·poly[d(AT)] a wrinkled D (wD) structure. These forms are grossly very similar to B- and D-DNA, respectively. In the wrinkled structures, the purine-to-pyrimidine step conforms essentially to standard B- or D-DNA, but the pyrimidine-to-purine step differs in a subtle way that leads to a wrinkling of the surface of the helices. The orientation of the phosphate groups in the 5′-pyrimidine-to-3′-purine steps is different (Arnott et al., 1983). An overall bending of the molecule seems to occur. In wrinkled B- and B-DNA, there are typically 10 base pairs per helical turn. Wrinkled D- and D-DNA are characterized by 8 base pairs per helical turn, a more pronounced base propeller twist, and a very narrow minor groove (Figure 1). The minor groove is deeper and the major groove is shallower than in B-DNA, giving the molecule a very overwound appearance.

Previous studies on $[d(AT)_5]_2$ (Suzuki et al., 1986) and $[d(GGTATACC)]_2$ (Zhou et al., 1987, 1988) in solution have suggested that the wrinkled D structure best accounted for the experimental 2D NOE spectra for the d(ATAT) moiety. In AT-rich sequences, methyl group hydrophobic interactions have been implicated by molecular mechanics calculations as promoting the wrinkled D structure. High-resolution solution studies of tracts of GCGC have not been done, but sugar conformational analysis on d(GCGC) and d(GCGCGC) by *J*-coupling analysis did not show any alternating structure (Cheung et al., 1984). Thus it is of interest to see what structure $d(AC)_4 \cdot d(GT)_4$ adopts. Indeed, recent studies (Rinkel et al., 1987) of chemical shift and coupling constant data for $[d(ACACGTGT)]_2$ have indicated an alternating rather than a regular structure for that oligomer.

Alternating tracts of GTG/CAC and TGTG/ACAC have been found with significant frequency in protein-binding domains of DNA (Lu et al., 1985), raising the question of a structure–function relationship. In the *lac* operon, for example, an associated maximum in the rate of the imino proton exchange occurs at a GTG/CAC sequence. The *lac* repressor

† This work was supported by National Institutes of Health Grants GM 39247, CA 27343, and RR 01695.

* Author to whom correspondence should be addressed.

‡ Present address: Applied Biosystems, Inc., Foster City, CA 94404.

0006-2960/90/0429-11161$02.50/0 

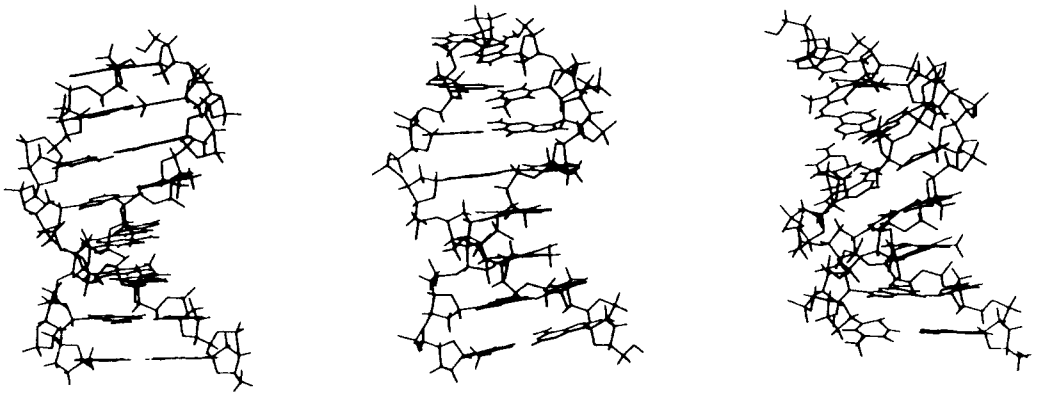

FIGURE 1: Pictorial representation of three DNA fragments from the B family: (from left to right) standard B, wrinkled B and wrinkled D. The sequence is $d(AC)_4 \cdot d(GT)_4$.

is known to bind poly[d(AT)·poly[d(AT)] more than 1000 times more strongly than a general sequence of DNA (Arnott et al., 1983), and alternating d(AT) sequences appear to be ubiquitous in the gene promoter sequence. The wrinkled secondary structure must have important implications for protein recognition and binding.

To date, a large number of DNA and RNA oligomers have been studied in varying detail by NMR solution methods (van de Ven & Hilbers, 1988). Analyses have varied from fairly qualitative NOE assessment of spectra (Chary et al., 1987), partial analysis (sugar pucker only) (Celda et al., 1989), and semiquantitative NOE analysis based on the assumption of a linear relationship between NOE intensity and internuclear distance at short mixing times (the isolated spin pair approximation) (Banks et al., 1989; Nilges et al., 1987) to complete relaxation matrix methods and molecular mechanics calculations (Boelens et al., 1989). Our study is the first to attempt to correlate the results obtained by both COSY and 2D NOE analysis. With proteins, many recent studies include structural constraints from *J*-couplings (torsional constraints) that significantly improve the convergence of the final structure. Of course, application of such constraints requires the assumption of a single conformer state, which cannot strictly be made in the case of nucleic acid structure. Thus it may not be possible to apply torsional constraints (specifically sugar puckers) during structure calculation for a DNA fragment. What we can do, however, is to use the calculated sugar puckers, in the context of the pseudorotation angle concept (Altona & Sundaralingham, 1972), from COSY to verify the accuracy of molecular dynamics simulations. What follows is an account of the experimental COSY and 2D NOE spectra for $d(AC)_4 \cdot d(GT)_4$ and an analysis using SPHINX (Widmer & Wüthrich, 1986), CORMA (Borgias et al., 1987; Borgias & James, 1988), MARDIGRAS (Borgias & James, 1990), and AMBER (Singh et al., 1986). Part of the completeness of this study includes a new method for more accurate intensity determination of NOE spectra, essential for accurate CORMA calculations. This is especially necessary in non-self-complementary DNA sequences of repeating units such as the above, where overlap is considerable. A simple method for quantitating overlapping peaks is introduced.

## Materials and Methods

The deoxynucleotide octamers d(GTGTGTGT) and d(ACACACAC) were synthesized according to methods previously described (Broido et al., 1984). Duplex formation was followed by monitoring the NMR spectrum of 6.90 mg of $d(AC)_4$ dissolved in 0.2 mL of phosphate buffer (100 mM sodium phosphate, 190 mM NaCl, 0.2 mM EDTA, pH 7.04) and 0.2 mL of $D_2O$. Aliquots of a similar solution of 7.40 mg of $d(GT)_4$ were added until the peaks corresponding to single-strand oligomer disappeared. The sample was lyophilized several times from $D_2O$ solution and finally dissolved in 99.96% pure $D_2O$. The resulting solution was 5 mM octamer duplex. 2D NOE studies were conducted on this sample. 2D NOE studies were also conducted on the same sample and buffer, with 90% $H_2O$ and 10% $D_2O$.

For the COSY spectra, a portion of the material was desalted on a Sephadex G-10 column and dissolved in a buffer containing 50 mM sodium borate and 0.2 mM EDTA at pH 7.91, to give a 2 mM solution of the octamer. A series of lyophilizations against $D_2O$ were done as before.

NMR spectra were run at 500 MHz on a GE GN500 equipped with an Oxford Instruments magnet and a Nicolet 1280 computer. All spectra were run at 20 °C. Pure absorption 2D NOE spectra were obtained by using the pulse sequence delay–90°–$t_1$–90°–$\tau_m$–90°–$t_2$ and the States method of phase cycling with alternating block acquisition (States et al., 1982). The 2D NOE spectra in $D_2O$ were recorded at four mixing times: 50, 100, 200, and 300 ms. A delay time of 10 s between scans was used to allow for full relaxation of the magnetization. The carrier frequency was set to the HDO position, and a spectral width of 4000 Hz was used. Thirty-two scans per $t_1$ value were collected; 460 FID's were collected in $t_1$ with 4K data points stored in alternate blocks in $t_2$. All data were transferred to a Sun workstation for processing with locally written software. During data processing, Gaussian filters (−7 Hz line broadening with a shift of 20%) were used in $t_1$ and $t_2$ for resolution enhancement. The $t_1$ FID was zero-filled to 2K data points prior to Fourier transformation to give an eventual 2K × 2K 2D spectrum with a digital resolution of 2 Hz/point. The phase-cycling scheme will remove contributions from multiple quantum coherences, except zero quantum coherence, from the spectra. Contributions from zero-quantum coherences are minimal in the spectra, particularly for mixing times ≥100 ms, since (a) relaxation will be largely complete for the zero-quantum coherence prior to signal acquisition and (b) the unresolved contributions from the inphase and antiphase components will mostly cancel in absorption phase spectra with this quantitation scheme; any significant contributions not canceling should lead to asymmetric peak shapes, which were not observed.

The 2D NOE spectra in $H_2O$ were recorded with the three-pulse sequence described above, with the third pulse replaced by a $13\bar{3}\bar{1}$ pulse centered on $H_2O$ for a null (Hore, 1983). A 200-ms mixing time was used with 8192 data points in $t_2$ and 380 points in $t_1$, collected for a spectral width of 10 kHz in both dimensions.

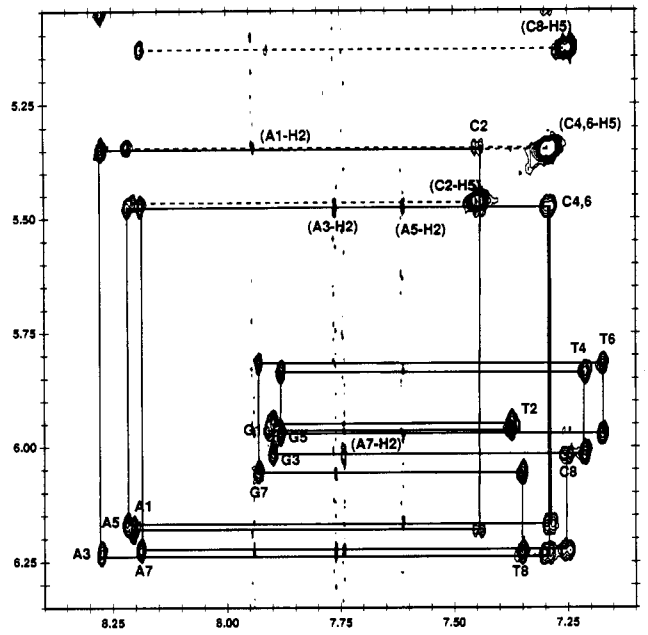


FIGURE 2: Part of the 200-ms 2D NOE spectrum of d(AC)$_4$·d(GT)$_4$ showing the aromatic proton (H6, H8) to H1′ cross-peaks. The method of assignment of the two chains by following the pathways from the H1′–same base NOE to the H1′–3′-neighboring base NOE is indicated. Also shown are the adenine H2 protons (for assignments, see text) and the cytosine H5′–cytosine H6 and cytosine H5–5′-neighboring adenine H8 interactions.

A pure absorption double-quantum-filtered COSY spectrum was recorded with the pulse sequence delay–90°–$t_1$–90°–$\tau$–90°–$t_2$, by using time-proportional phase incrementation (Drobny et al., 1979; Marion & Wüthrich, 1983) for separation of ±1 quantum transitions; $\tau$ was set to 5 $\mu$s. A spectral width of 4000 Hz in $t_2$ and 8000 Hz in $t_1$ was used, with a repetition time of 4 s. Sixty-four scans were averaged per $t_1$ value; 634 FID's were recorded in $t_1$ and 4K points in $t_2$. During data processing, a Gaussian filter was used in $t_2$ and a sine-bell filter (30°) in $t_1$. The $t_1$ FID was zero-filled to achieve a final 2K × 2K spectrum.

## Results and Discussion

### *Resonance Assignments*

Resonance assignments of all the protons in d(AC)$_4$·d(GT)$_4$, except for the H5′ and H5″ protons, were made from the 200-ms 2D NOE spectra, by analysis of the base → H1′, base → H2′,2″, and imino → amino + adenine H2. In the following discussion, the numbering and labeling of d(AC)$_4$·d(GT)$_4$ residues are

5′ — A1 C2 A3 C4 A5 C6 A7 C8 — 3′

3′ — T8 G7 T6 G5 T4 G3 T2 G1 — 5′

Figure 2 illustrates the method of assignment on the base–H1′ region and also indicates spectrum quality. Details of the assignment procedure are standard (Scheek et al., 1984; Broido et al., 1984; Wemmer et al., 1984) and are not repeated here.

The only ambiguity was in the assignment of the adenine H2 protons. For a fully relaxed spectrum, small cross-peaks between A-H2 and the 3′-neighboring C-H1′ proton were observed. Thus A1-H2 and A7-H2 could easily be assigned (Figure 2), but A3-H2 and A5-H2 could not be distinguished because of the complete overlap of C4- and C6-H1′. (Indeed, the C4 and C6 protons overlapped everywhere in the spectrum.) This ambiguity could be resolved from the imino proton

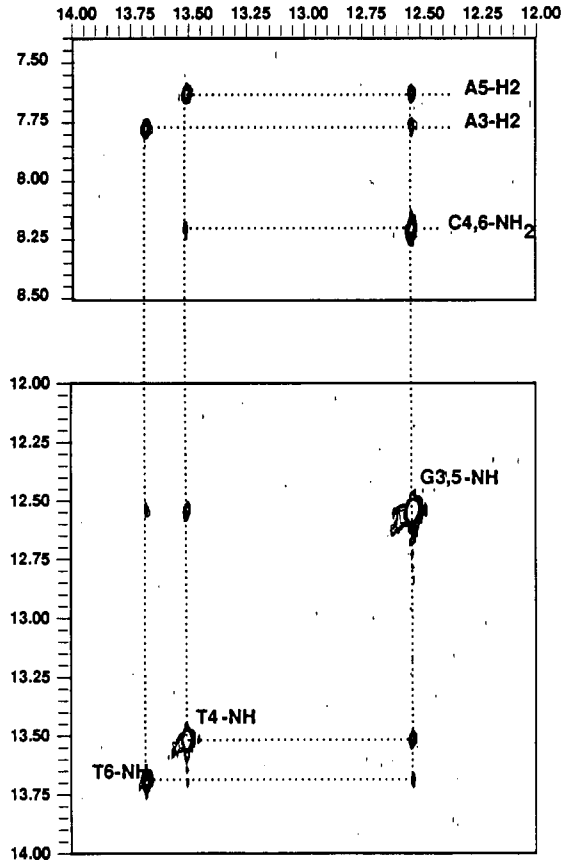


FIGURE 3: Part of the 200-ms NOE spectrum in $H_2O$ of d(AC)$_4$·d(GT)$_4$ showing cross-peaks in the imino proton to amino and adenine H2 proton region of the spectrum.

Table I: Proton–Proton Distances (Å) Appropriate to Analysis of Figure 3

| $^1$H–$^1$H distance[a] | B | wD | wB |
|---|---|---|---|
| C4 amino–T4 amino | 4.64 | 3.74 | 3.64 |
| C4 amino–T6 amino | 4.51 | 5.46 | 5.40 |
| T6 amino–A3-H2 | 2.90 | 2.76 | 2.97 |

[a] Base-pair hydrogen-bond protons.

connectivities in the $H_2O$ 2D NOE spectrum. In fact, the $H_2O$ 2D NOE provided a characteristic fingerprint for wrinkled DNA as opposed to smooth B-DNA.

### *A Characteristic 2D NOE Pattern for Wrinkled DNA*

Figure 3 shows the imino (T-N3H; G-N1H) proton region of a 200-ms 2D NOE spectrum taken in 90% $H_2O$ and 10% $D_2O$. Connectivities to A-H2 and C-$NH_2$ are also shown. All G-$NH_2$ protons and terminal residue imino and amino protons were exchanging rapidly under the conditions of the experiment and were not observed. Expected NOE couplings between T-N3H and A-H2 of a base pair are observed, as well as couplings between G-N1H and C-$NH_2$ of a base pair. The break in the symmetry of the NOE pattern comes in the observation of a connectivity between only one of T4- and T6-N3H and C4- or C6-$NH_2$. It allows the assignment of T4-N3H, T6-N3H, A3-H2, and A5-H2 and unequivocally verifies the existence of an alternating structure for d(AC)$_4$·d(GT)$_4$ characteristic of the wrinkled B or wrinkled D forms. Table I shows the expected distances for T-N3H–C-$NH_2$ across the chain. Clearly the asymmetry in different directions along the chain is marked for wrinkled structures (wD and wB). A C4 amino–T4 imino cross-peak is expected but not a C4 amino–T6 imino cross-peak. Hence the as-

signments shown in Figures 2 and 3 are made. In B-DNA, peaks of the intensity observed would not be expected in either direction (Wüthrich, 1986).

*DQF-COSY Spectra*

Double-quantum-filtered COSY spectra (DQF-COSY) of $d(AC)_4 \cdot d(GT)_4$ were obtained for a 2 mM solution in 50 mM borate. These low concentration, low salt conditions were found to enhance the resolution of the spectra obtained. The chemical shifts were identical with those from the 5 mM octamer solution in 100 mM phosphate and 190 mM NaCl, the conditions used for the 2D NOE spectra. Assignments made with the 2D NOE spectra were confirmed. Three regions of the spectrum were analyzed to determine the vicinal coupling constants between sugar protons, in an attempt to determine the sugar pucker for each nucleotide (Rinkel & Altona, 1987). The 1′2′ and 1′2″ region, its diagonally opposite 2′1′ and 2″1′ region, and the 3′2′ and 3′2″ region were simulated by using SPHINX and LINSHA (Widmer & Wüthrich, 1986; Celda et al., 1989).

In general, it is very difficult to directly extract numerical values of the $J$-couplings in macromolecules from COSY antiphase peaks because of the large inherent line widths compared to the scalar coupling constant $J$. ECOSY (Griesinger et al., 1985) has been introduced as a method to obtain $J$-couplings by eliminating all indirect transitions and hence removing distorting overlap. We found that measuring $J$-couplings by ECOSY was limited to an accuracy of ±1 Hz because of broad lines and limited digital resolution. Thus ECOSY could not provide a list of $J$-couplings that could be used to accurately interpret sugar pucker. We note, however, that the PCOSY experiment recently described by Marion and Bax (1988) could provide an attractive alternative. The power of the SPHINX method, which could be applied to PCOSY as well as DQF-COSY, lies in its ability to extract coupling constant information from peak intensity patterns without the necessity for observable resolution of scalar splitting. An exact simulation of a complex DQF-COSY cross-peak lends confidence to the results obtained (Schmitz et al., 1990). This is particularly true because the cross-peak patterns are very sensitive to the parameters involved, namely, vicinal and geminal coupling constants, line width, line shape, filter functions applied, acquisition times, digital resolution, and phase. The experimental parameters are known of course, and it is the coupling constants that we are trying to evaluate. There are six of these and six peaks to simulate. The chief stumbling block is in establishing the correct line width as will be shown below. A line width too small can be compensated by increasing $J$ and vice versa. This can result in uncertainty in the final solution and leads, in the case of $d(AC)_4 \cdot d(GT)_4$, to two possible solutions for the purine sugar coupling constants (vide infra).

The (1′,2′, 1′,2″), (2′,1′, 2″,1′), and (3′,2′, 3′,2″) regions of the spectrum are shown in Figure 4. Qualitatively, an immediate distinction between purines and pyrimidines can be seen from the appearance of the 1′2′ cross-peak [as well as from significant differences in the H2′ and H2″ chemical shifts (Rinkel et al., 1987)]. Sample pyrimidine (C2) and purine (A3) cross-peaks appear with greater magnification in Figure 6 (vide infra). Their 1′2′ peaks are quite different (and hence $J_{1'2'}$, $J_{1'2''}$, and $J_{2'3'}$). Yet the other peaks are not as obviously different. To correctly ascertain sugar conformation, it is important to be able to simulate all of the DQF-COSY spectral features. In what follows, the 3′2′ peaks were used only for testing and not for fitting, because of a very overlapped purine 3′2′ region.

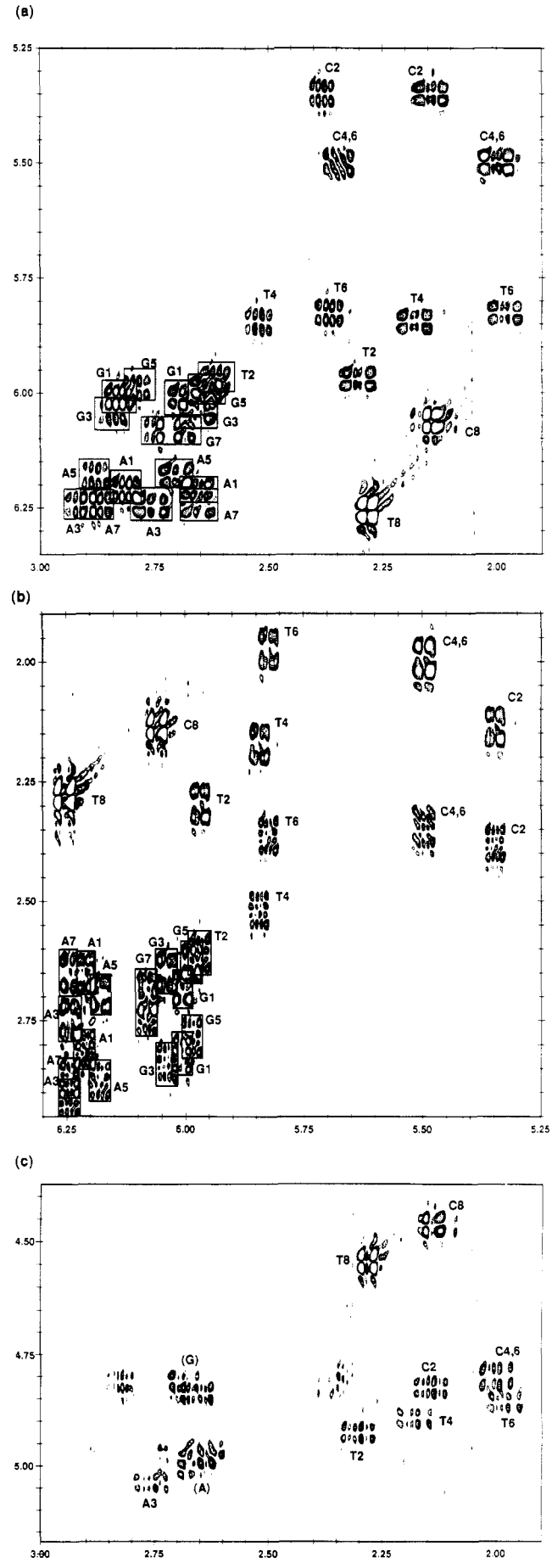


FIGURE 4: Part of the double-quantum-filtered COSY spectrum of $d(AC)_4 \cdot d(GT)_4$ showing (a) the H2′,H2″–H1′ region, (b) the H1′–H2′,H2″ region, and (c) the H2′,H2″–H3′ region.

The terminal nucleotides are considerably frayed, and their puckering is altered by this end effect. The terminal pyrimidines have overlapping 2′ and 2″ protons. They are not considered further in this investigation.

*Defining the Line Width.* As it is crucial for determination of the coupling constants, we examined the dependence of peak pattern on line width for the 2′1′ and 2″1′ cross-peaks, assuming a sugar pseudorotation angle **P** of 180° (see supplementary material). These peaks were chosen in an attempt to define the line width because of their similarity for all nucleotides in the experimental spectra. The line widths tested were taken from previous studies (Celda et al., 1989; Schmitz et al., 1990).

*The H1′ Line Width.* The 2′1′ peak is especially useful for establishing the line width of the 1′ proton. In the experimental spectra, there are four intense outer peaks with obvious tails. These four peaks are partially split inphase along $\omega_2$ (H1′) by passive couplings. This effect is seen for both purines and pyrimidines and is thus not solely dependent on the size of the couplings. We found this splitting to occur when the H1′ line width is reduced below ~7 Hz (see supplementary material). So 6 Hz was chosen to represent the H1′ protons.

*The H2′ Line Width.* The H2′ and H2″ line widths were deduced from the appearance of the 2′1′ and 2″1′ peaks in Figure 4, taking into account the fairly significant effect of pseudorotation angle **P** (shown in Figure 5). The intense tailing of the 2′1′ peak along $\omega_1$ that occurs on decreasing the line width and also on increasing **P** was not observed in the experimental peaks. This led us to choose the larger line width of 9 Hz for the H2′ protons. Later we will show that an even larger line width of 11 Hz might be more appropriate for the purine H2′ protons.

*The H2″ Line Width.* The H2″ line width is clearly less than the H2′ line width. In all experimental spectra, a 16-peak pattern was obtained for the 2″1′ peak. However, use of a 9-Hz line width for the 2″ proton led to the disappearance of the outer peaks along the third row (see supplementary material) for all values of **P** between 99° and 225°. At an H2″ line width of 8 Hz, these peaks reappeared, so 8 Hz was chosen.

*Pyrimidines Can Be Described by a Single Conformer (**P** = 144°).* Figure 5 shows a series of simulations of the 1′2′, 1′2″, 3′2′, 3′2″, 2′1′, and 2″1′ cross-peaks as a function of pseudorotation angle **P**, assuming a pucker amplitude of 35° (Rinkel & Altona, 1987). The line widths were chosen as described above. Other parameters kept constant were $J_{2'2''}$ = −14 Hz (−15 Hz tested worse in all cases) and $J_{3'P}$ = 5.8 Hz. For pyrimidines, an average value for the chemical shift difference $(\nu_{2''} - \nu_{2'})$ = 143 Hz was used. The characteristic inner peak pattern observed for the 1′2′ peak of all pyrimidines is reproduced at **P** = 144°. All other peaks match well with this value of **P** (Figure 9). Calculations of mixtures with various proportions of N and S conformers with **P** = 9° for the N conformer and **P** = 144°, 153°, or 171° for the S conformer could not reproduce the 1′2′ peak.

*Purines Can Be Described by a Single Conformer (**P** = 180°) or by a Conformer Mix: 85% S (**P** = 153°) and 15% N (**P** = 9°).* No match can be found for the purine DQF-COSY peaks from Figure 5. To fit the 1′2′ peak, a very high **P** (>207°) is required. However, this clearly gives a very poor fit of the other peaks in the spectrum. An attempt to fit the purines with a mixture of S (**P** = 144°) and N (**P** = 9°) conformers produced no better results. The 1′2′ peak could only be reproduced at >40% N, but the 2″1′ peak could only be reproduced at <10% N. Consequently, two approaches

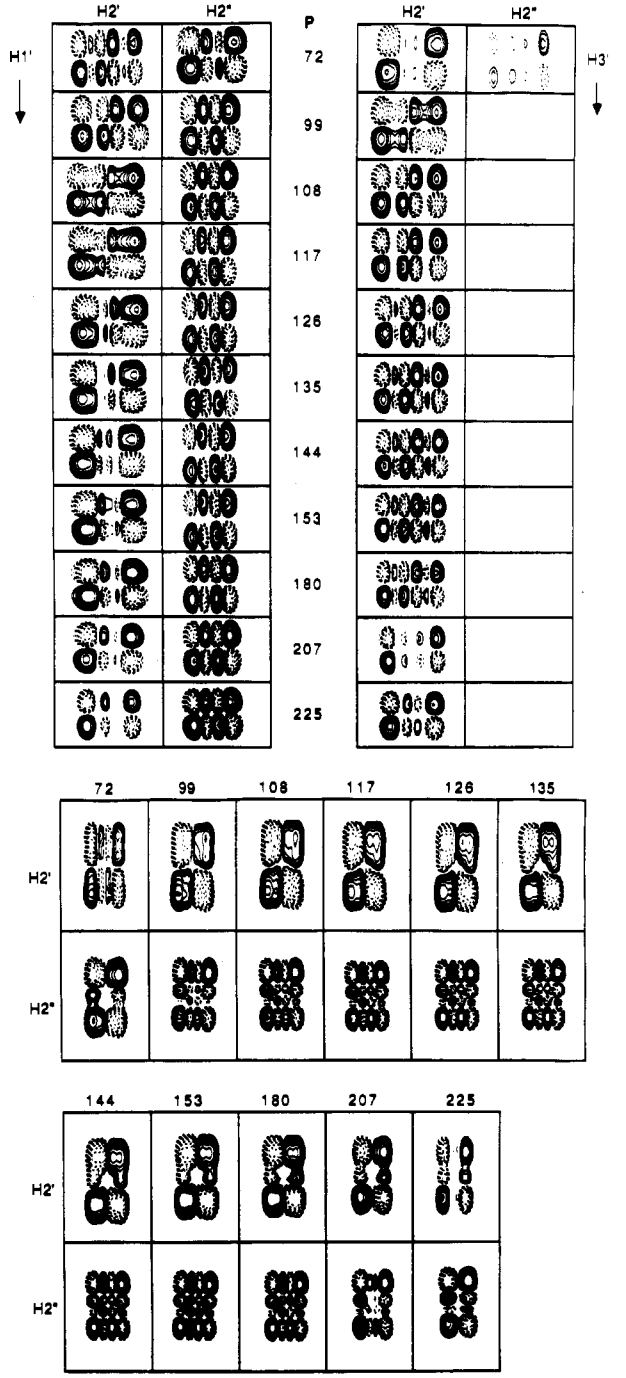


FIGURE 5: Simulation of the DQF-COSY cross-peaks for d(AC)$_4$·d(GT)$_4$ as a function of pseudorotation angle **P**. $\omega_1$ is vertical and $\omega_2$ horizontal. Shown are the H1′–H2′,H2″, H3′–H2′,H2″, and H2′,H2″–H1′ cross-peaks. Line widths used in the simulation are given in the text. Also used were $\nu_{2'} - \nu_{2''}$ = 142 Hz, sin 67.5° filter function in $\omega_2$, sin 30° filter function in $\omega_1$, and acquisition times and digital resolution as used with experimental data.

were employed for the evaluation of the purine sugar pucker.

(1) The 1′2′, 2′1′, and 2″1′ peaks were simulated for values of $J_{2'3'}$ = 8.4, 7.4, 6.6, 6.2, and 5.6 Hz and values of $J_{1'2'}$ = 11.0, 10.2, 9.0, 8.0, 7.0, 5.9, and 5.0 Hz. $J_{2'2''}$ = −14.0 Hz and −15.0 Hz were both tried, with the latter giving poorer fits. $J_{2''3'}$ was taken as 1.2 Hz. $J_{1'2''}$ = 6.8 and 5.7 Hz were tried with little change. The chemical shift difference $(\nu_{2''} - \nu_{2'})$ = 82.5 Hz was used as a good representation for most purines. The 2″1′ peak was also followed in a map of $J_{1'2''}$ = 5.6, 6.4, 7.5, and 8.4 Hz and $J_{2''3'}$ = 4.4, 3.75, 2.5, and 1.2 Hz, keeping $J_{1'2'}$ = (a) 8.0 Hz and (b) 7.0 Hz and $J_{2'3'}$ = 6.5 Hz.

A sample of these simulations is included in the supple-

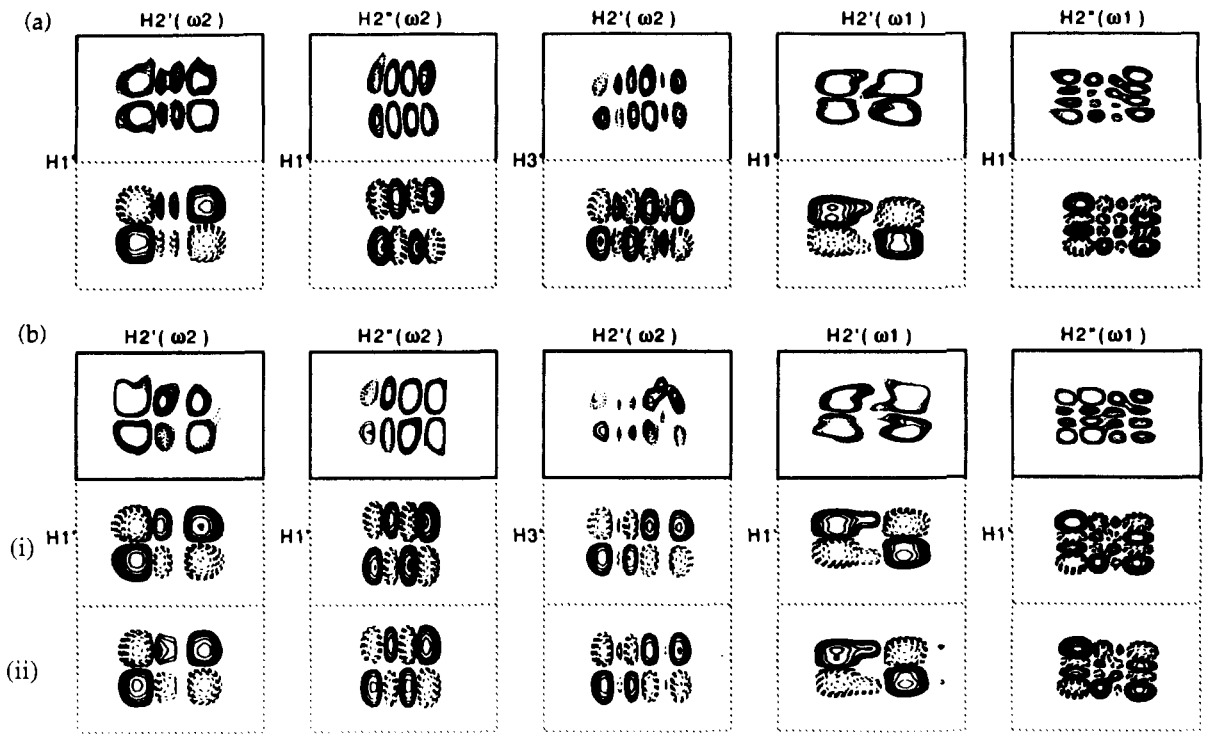


FIGURE 6: Best fit simulations of the (a) pyrimidine (C2) and (b) purine (A3) DQF-COSY cross-peaks. The pyrimidine simulation corresponds to a single sugar pucker of **P** = 144°, with $J_{2'2''}$ = −14 Hz, $\nu_{2'} - \nu_{1'}$ = 142 Hz, and line widths H1′ = 6 Hz, H2′ = 9 Hz, H2″ = 8 Hz, and H3′ = 6 Hz. The purine simulations correspond to (i) a single sugar pucker of **P** = 180°, with $J_{2'2''}$ = −14 Hz, $\nu_{2'} - \nu_{1'}$ = 82.5 Hz, and line widths H1′ = 6 Hz, H2′ = 11 Hz, H2″ = 8 Hz, and H3′ = 6 Hz, and (ii) a mixture of 15% N (**P** = 9°) and 85% S (**P** = 153°), with $J_{2'2''}$ = −14 Hz, $\nu_{2'} - \nu_{1'}$ = 82.5 Hz, and line widths as for the pyrimidines.

mentary material. Regions that match experimental peaks were noted, and a search was made for selected areas of *J*-couplings that overlap. Not much overlap occurs, allowing a narrow range in the selection of the coupling constants. The following conclusions could consequently be drawn:

$$9.0 \text{ Hz} \geq J_{1'2'} > 8.0 \text{ Hz}$$

$$6.2 \text{ Hz} \leq J_{2'3'} \leq 6.6 \text{ Hz if } J_{2'2''} = -1.4 \text{ Hz}$$
$$\leq 7.4 \text{ Hz if } J_{2'2''} = -15 \text{ Hz}$$

$$J_{1'2''} \leq 6.4 \text{ Hz}$$

$$J_{2''3'} \leq 2.5 \text{ Hz if } J_{1'2''} \leq 6.4 \text{ Hz}$$
$$\leq 3.7 \text{ Hz if } J_{1'2''} \leq 5.6 \text{ Hz}$$

A search of two-conformational space was made to fit these regions of $J_{ij}$. Mixtures of N (**P** = 9°) and S (**P** = 144°, 153°, 162°, and 171°) were tried, to fit the equation

$$J_{ij} = J_{ij}^{N}(1 - p_S) + J_{ij}^{S}p_S$$

where $p_S$ is the population of the S conformer and $J_{ij}^{N}$ and $J_{ij}^{S}$ are the coupling constants for the pure N and S conformers. Several possibilities were tested by simulation. The conditions were best met for a 15/85 (±5) mixture of N (**P** = 9°) and S (**P** = 153°).

(2) When the line width of the H2′ protons of the purines was increased to 11 Hz, a straightforward and simple fit to a single S conformer with **P** = 180° was obtained. This is at least as good as that obtained from a two-conformer model. The line-width effect might be explained by a different local environment for the pyrimidines and purines.

Figure 6 shows the comparison of experimental and calculated DQF-COSY cross-peaks for pyrimidines and purines. Table II gives the *J*-couplings determined by this simulation fo the DQF-COSY spectra. We point out here that the guanosine cross-peaks are so overlapped that it is impossible to obtain separate information on their sugar puckers. It is only assumed here from the similarity of cytidine and thymidine cross-peaks that the guanosine sugars are similar to the adenosines.

Table II: Sugar Ring Vicinal Coupling Constants (Hz) Determined from DQF-COSY

| | | purines[b] | |
|---|---|---|---|
| $J_{ij}$[a] | pyrimidines | 1 | 2 |
| $J_{1'2'}$ | 10.2 ± 0.1 | 8.9 ± 0.5 | 9.4 ± 0.4 |
| $J_{1'2''}$ | 5.6 ± 0.1 | 6.0 ± 0.2 | 5.8 ± 0.2 |
| $J_{2'3'}$ | 6.6 ± 0.4 | 6.3 ± 0.1 | 5.5 ± 0.1 |
| $J_{2''3'}$ | 1.2 ± 0.1 | 2.5 ± 0.4 | 1.3 ± 0.1 |
| $J_{3'4'}$ | 2.3 ± 0.4 | 2.7 ± 0.3 | 1.0 ± 0.1 |

[a] $J_{2'2''}$ = −14 Hz; $J_{3'P}$ = 5.8 Hz. [b] (1) For an 85/15 S/N mixture (see text); (2) for a single conformer, **P** = 180° (see text).

*Comment on Observation of Pure Conformational States.* Previous papers (van de Ven & Hilbers, 1988; Rinkel & Altona, 1987) have suggested that a static model with a single sugar conformation for each nucleotide is inadequate to describe experimental *J*-couplings. While it is quite clear (from energetic considerations and molecular dynamics films) that oligomers are in a state of considerable dynamic flux, it is not apparent that they cannot be described by a single time-averaged conformation. We wish to argue that insufficient data have been collected to unequivocally show that NMR data cannot be explained by a single time-averaged conformer. Most of the studies to date were conducted on small nucleotide duplexes (≤4 base pairs) or on single strands, where line widths were small enough for *J*-couplings to be extracted by one-dimensional simulations on idealized line shapes. It is also known that terminal nucleotides display extreme conformational flexibility, so that short duplexes are not good examples to study. The current study and other studies using SPHINX (Celda et al., 1989), which simulates the effect of filter functions, truncation, and line widths on 2D multiplets, show that a pure conformational state for each nucleotide can ad-

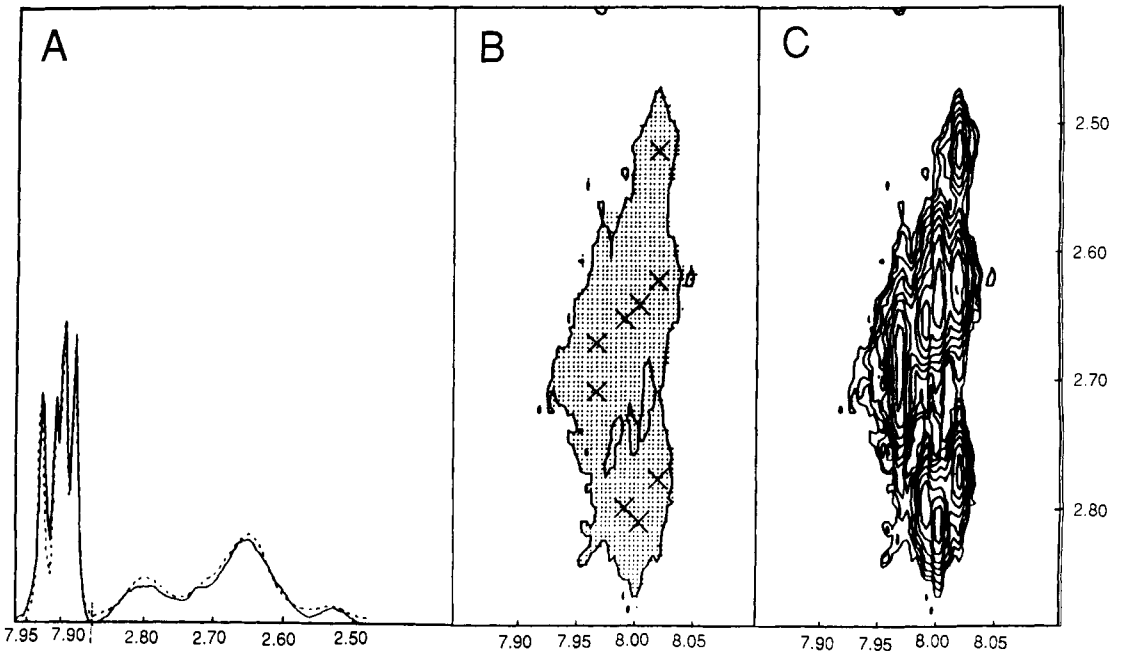


FIGURE 7: An example of the contour fitting method of integrating peaks in a 2D NOE spectrum applied to the G-H8–H2′,H2″ region of the spectrum. The shaded area corresponds to pixels that are added to determine peak intensity. In the case of multiply overlapped peaks (panel C) (indicated by crosses within the closed contour in panel B), a simulation of the $x$ and $y$ projections of the closed contour is carried out to determine the contribution of the component peaks (panel A). The fit is indicated by a comparison of the experimental (—) and simulated (- - -) $x$ and $y$ projections. In the example shown, peaks were simulated with a 6-Hz line width along $x$ (H8 protons) and a 28-Hz line width along $y$ (H2′,H2″ protons).

equately explain the $J$-couplings. However, two-state models cannot be ruled out as another possible solution. In fact, energetic and dynamic calculations suggest multiple states are populated, so the commonly employed two-state model is probably not an accurate reflection of reality either. An attempt to adequately describe all experimental parameters in terms of a single conformation for each sugar is to find a time average of the dynamic structure. An analysis in terms of a two-state model simply reminds us that there is in reality a dynamic conformational equilibrium.

### *2D NOE Spectra*

*Quantifying Peak Intensities.* The NOE intensities need to be accurate for a quantitative interpretation of 2D NOE spectra by a program such as CORMA. Several regions of the spectrum are significantly overlapped, e.g., the purine H8–H2′,H2″ region, shown in Figure 7. It is difficult to imagine extracting accurate intensities from these regions by boxing (Zhou et al., 1987) or circling (Boelens et al., 1989) individual peaks or by simulating selected slices through the peaks (Broido et al., 1985). More exact NOE intensity measurements have been described. Peaks with known line widths and $J$-coupling fine structure can be simulated for greater accuracy (Weiss & Ferretti, 1983), but this is a difficult and time-consuming procedure, since the parameters are not always known. An interesting method has been developed for deriving an intensity vector from an NOE spectrum (Denk et al., 1986). The intensity vector is obtained by several multiplication and inversion steps between the original data and a matrix of reference lines for all protons. The elements of the matrix represent the intensities of the NOE transitions between all proton pairs. The difficulty with this method is in obtaining a reference line matrix, which again requires knowledge of $J$ and line width. If, as suggested, experimental reference lines are extracted from the original spectrum, the method is time-consuming, prone to accumulation of noise, and dependent on finding a well-resolved resonance for every proton. Nevertheless, a demonstration of the method on a 17-residue polypeptide was recently shown (Olejniczak et al., 1989).

The intensity measurement program used here is semiautomatic and simple to use. The first step is to locate and identify all the peaks in a given region and to define a line width for each proton resonance. The intensity of a region (containing one or more peaks) is then quantitated by adding up the signal inside a base contour drawn as close to the noise level as possible. For overlapping peaks, the relative contribution of each component peak is determined by simulating and fitting the $x$ and $y$ sum projections of the region. For the simulation, the user-provided line width is used as well as the line shape known from the way in which the data were manipulated and transformed, assuming an original Lorentzian decay. An example of the results of this procedure is shown in Figure 7.

Knowledge of the $J$-couplings is not required. It is left to the user to know whether two or more peaks in an overlapped region belong to the same proton. Accurate representation of the line width is important for accurate intensity measurement. The correctness of the chosen line widths can often been seen by gauging the exactness of the fit of experimental and calculated $x$ and $y$ projections and adjusting accordingly. At present, the simulation does not include the possibility of varing the individual line widths, but that would improve the method. The chief error arises from underestimating the intensity due to inevitably choosing a base contour slightly above the noise level. This error can be minimized by using a Gaussian filter to reduce the tails of the peaks. Figure 8 shows the results of calculations that demonstrate the reduction in measured intensity as a function of (a) the amount of base neglected in the measurement, as a percentage of the peak height, and (b) signal to noise (assuming the base cut is made exactly at the upper tip of the noise level). Figure 8 was calculated with a digitized simulated Lorentzian FID to which Lorentzian or Gaussian apodization was applied to achieve a particular line width. It is clear that the intensity falloff is considerably curtailed for a Gaussian-shaped peak compared to a Lorentzian. It is evident that considerable intensity is lost

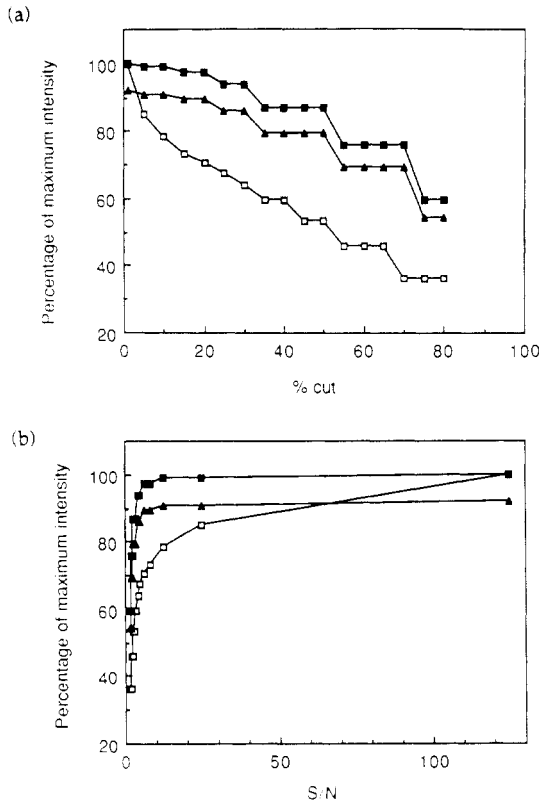


FIGURE 8: Calculation of the measured intensity as a function of (a) the extent to which the lowest contour chosen for quantitation is above the true base line, expressed as a percentage of the peak height, and (b) the signal to noise of the peak, assuming that the base contour cut is made precisely at the upper tip of the noise. The effect is shown for Lorentzian- (□) and Gaussian-shaped (■) peaks, assuming 100% intensity for zero noise, and also for a Gaussian-shaped peak (▲) with intensity relative to the total Lorentzian intensity.

due to the Lorentzian tail. It is also apparent in comparing the intensity of the signal one would obtain using our deconvolution technique on a Gaussian-apodized signal to that of the unapodized Lorentzian peak that we will still have ca. 8% reduction in signal intensity even at higher signal-to-noise values. If we are willing to accept this level of error, then peaks with a signal-to-noise ratio as low as 5 can be integrated with an error <10%.

Figure 9 compares intensities derived by this method versus an alternative method of boxing individual peaks, which is similar to that employed in a number of programs currently in wide use. While isolated peaks typically give an intensity slightly higher (≤10%) than that obtained by the new method, overlapped peaks are typically incorrectly estimated by the boxing method, some being represented too high and others much too low.

*Selection of NOE Cross-Peaks.* By use of the intensity measurement procedure described above, 140 2D NOE cross-peaks in each spectrum were quantitated; spectra obtained with the octamer duplex in $D_2O$ solution at the four mixing times 50, 100, 200, and 300 ms were examined. However, only 109 distances resulting from this quantitation were subsequently utilized in structure analysis. These were from base to H1′, H2′, H2″, H3′, and H4′ cross-peaks and intrasugar cross-peaks. Fixed distances, such as between geminal protons and between C-H5 and C-H6, were not utilized. An additional 16 distances to methyl groups were excluded from quantitative analysis because of the uncertainties in defining their motion. There were also a few more excluded that were derived from badly overlapped peaks and were consequently deemed less reliable. Exchangeable proton

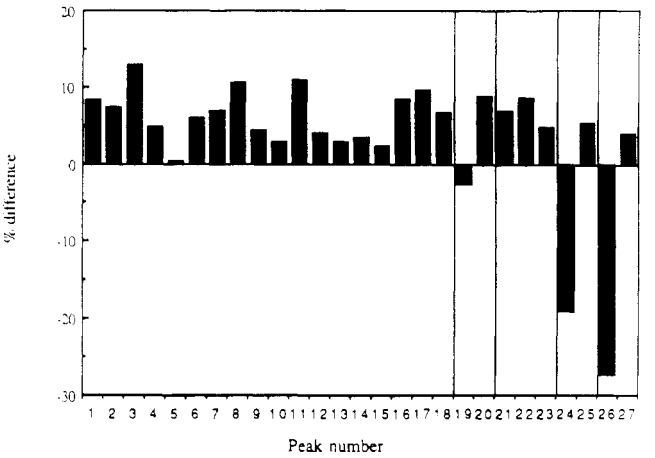


FIGURE 9: A selection of peaks showing a comparison of the contour integration method of simulating overlapped peaks vs a method by which peaks are individually boxed and integrated. The percent difference is given by $(I_{box} - I_{sim})/I_{box}$, where $I_{box}$ is the intensity obtained by boxing and $I_{sim}$ that obtained by simulation or contouring. The techniques agree fairly well for isolated peaks, with the slight loss in intensity due to nonzero base contour cut obvious. For four sets of representative overlapped peaks (drawn to the right of the bar graph and delineated by vertical lines), where a base line cannot be adequately determined for boxing, discrepancies in the relative contributions of components of an overlapped region occur.

cross-peaks were excluded because of intensity distortion due to use of the $13\bar{3}\bar{1}$ pulse.

*Correlation Time.* Cross-peak intensities are a function of internuclear separations, averaged by molecular motions, and of correlation times. The overall tumbling motion in the nearly spherical hydrated octamer should be effectively isotropic, and it can be described by a single correlation time. Also, with the exception of methyl rotation, internal motions are on the order of a nanosecond or slower, so it is not an unreasonable approximation to treat all proton–proton dipolar interactions as having a single isotropic correlation time (Keepers & James, 1984). In the following paper, the 2D NOE peak intensities are analyzed quantitatively in an attempt to describe a time- and ensemble-averaged conformation. Using constrained molecular dynamics, we studied the extent to which we can follow conformational fluctuation.

A correlation time $\tau_c = 2$ ns for the octamer was used. This was derived from the equation relating the spin–lattice ($T_1$) and spin–spin ($T_2$) relaxation times to $\tau_c$, with the approximation of no spin diffusion (Suzuki et al., 1986):

$$\tau_c = \frac{2}{\omega}\left(\frac{3T_2}{T_1}\right)^{-1/2}$$

where $\omega$ is the spectrometer operating frequency in radians. The value of 2 ns for $\tau_c$ was calculated for the four adenine H2 protons, which are well-resolved singlets in the spectrum. $\tau_c$ was also calculated for adenine H8, resulting in a value of 3 ns. Spin diffusion is a much more likely contributor to H8 and will tend to make $\tau_c$ too long. Dissolved oxygen could, on the other hand, make $\tau_c$ for the H2 protons too short. All things considered, the choice of correlation time utilized seems reasonable. We did carry out a MARDIGRAS analysis of the peak intensities utilizing a value of 3 ns for $\tau_c$ (cf. following paper) and found that the change in correlation time changed internuclear distance determinations by <10% (<1% for the majority of distances).

CORMA *Reflects the Alternating Structure of* $d(AC)_4 \cdot d(GT)_4$. NOE spectra were analyzed with a complete relaxation matrix approach, CORMA (Keepers & James, 1984; Borgias

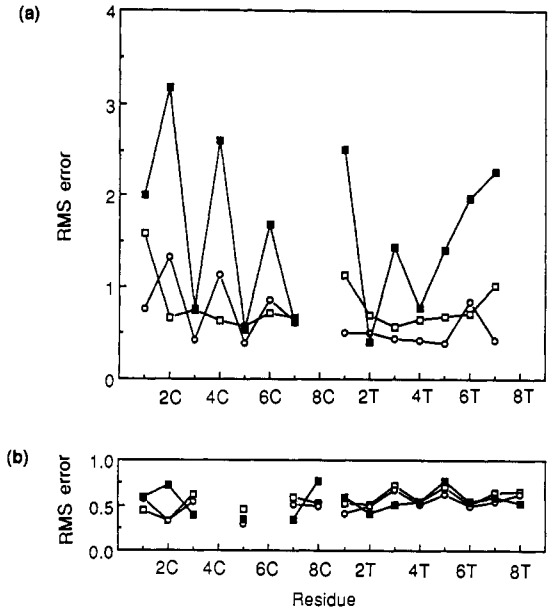


FIGURE 10: Root mean square deviation of observed NOE intensity to calculated intensity for three structures, standard B- (■), wB- (○), and wD-DNA (□). The RMS error is given by $(\sum_n[(I_o - I_c)/I_o]^2/n)^{1/2}$, where $I_o$ is the observed intensity, $I_c$ is the calculated intensity, and $n$ is the number of observed intensities. Part a shows interresidue NOE errors, and part b shows intraresidue deviations. In (a), data shown at residue position $m$ imply the $m \rightarrow m + 1$ interresidue interactions in the 5′ → 3′ direction along the chain.

& James, 1988). The program CORMA, which calculates theoretical 2D NOE peak intensities accounting for all proton dipole–dipole interactions for any assumed structure, was run for the various mixing times with different starting structures: B-, wB-, and wD-DNA. B-DNA is the standard Arnott B-form. Structures for wB- and wD-DNA were determined from coordinates given by Arnott et al. (1983) for polymeric d(GC)$_n$ and d(AT)$_n$, respectively, by appropriate base modification using MIDAS (Jarvis et al., 1986), followed by energy minimization using AMBER (Singh et al. 1986). The experimental intensities were normalized by a scaling factor $s$ determined from the ratio of calculated and experimental intensities for fixed proton distances:

$$s = \sum a_{ij,\mathrm{calc}} / \sum a_{ij,\mathrm{exp}}$$

Figure 10 shows the RMS deviation between calculated and observed intensities as a function of residue number. There were typically 7–13 observed NOE's per residue, except for the terminal residues that had 5–7 observed NOE's and the cytosine residues C4 and C6 that were completely overlapped in the spectrum and yielded no intraresidue contacts and only 3 interresidue contacts. Figure 10a shows the RMS deviation for interresidue contacts, and Figure 10b shows the RMS deviation for intraresidue contacts. For comparison of the three structures, B, wD, and wB, interresidue contacts prove to be a sensitive gauge of structure. Along the d(AC) chain, B is clearly the worst structure and wD the best. The oscillations evident in the curve for the B structure show that the NOE contacts for the purine-to-pyrimidine step are well represented by the B structure but that the pyrimidine-to-purine steps are far off. This is precisely what we would expect to find for a wrinkled structure. The data for the d(GT) chain are less clear; in fact, wD is not a better representative of the structure than wB. It appears that the NOE data are indicating a certain asymmetry between the chains. Figure 11 shows the deviation for specific interactions between calculated and observed intensity ($I_{\mathrm{calc}} - I_{\mathrm{obs}}$) for each of the three

Table III: Sugar Puckers and Amplitudes for B-Type DNA Duplexes

| | B | wB | wD | d(AC)$_4$·d(GT)$_4$ |
|---|---|---|---|---|
| | | Puckers (deg) | | |
| purine | 171 | 178 | 178 | 180 ± 10 |
| pyrimidine | 171 | 161 | 152 | 144 ± 6 |
| | | Amplitudes (deg) | | |
| purine | 35 | 43 | 44 | 35 |
| pyrimidine | 35 | 53 | 44 | 35 |

structures. The pertinent interactions are between base and intranucleotide sugar, base and 5′-neighboring sugar, and intrasugar protons. Data at different mixing times gave results quite similar to the 100-ms data shown. A striking oscillation in the intensity deviation is seen on moving from pyrimidine to purine throughout the chain. The effect is most marked for the B-DNA model, clearly indicating a deviation from regular B-DNA and qualitatively confirming an alternating or wrinkled structure.

The wrinkling effect is pronounced for the following NOE interactions: (a) intranucleotide base proton (H6 or H8) to H2′, (b) H1′–H4′, and (c) internucleotide base proton (H6$_{n+1}$ or H8$_{n+1}$) to H2″$_n$. The largest alternations are seen for the NOE's with the closest proton distances, since these are the most sensitive to small changes. The large intraresidue base–H2′ and small interresidue base–H2′ NOE's immediately identify d(AC)$_4$·d(GT)$_4$ as a member of the B family (van de Ven & Hilbers, 1988). The alternating nature of B-like d(AC)$_4$·d(GT)$_4$ is also immediately apparent from these NOE's.

Intranucleotide distance constraints such as base proton–H2′ are a function of three degrees of conformational freedom, namely, pseudorotational parameters **P** and $\phi_m$ and glycosidic torsion angle $\chi$. Interresidue NOE's such as base–H2″ depend, of course, on all backbone angles and sugar pucker or alternatively on helix twist, roll, rise, etc. The H1′–H4′ distance reflects sugar pucker **P** with extreme sensitivity and thus also backbone torsion angle $\delta$. The H1′–H4′ NOE cross-peaks are an extremely useful way of defining sugar pucker, provided the effects of spin diffusion are taken into account, as they are with CORMA and, as we shall see shortly, with the MARDIGRAS procedure (Borgias & James, 1990).

The CORMA calculations on standard wB and wD models (Figure 11b,c) show reduced oscillations, as would be expected if these wrinkled structures more closely approximated the actual structure. There is a remarkable improvement for both wB and wD in the intranucleotide base–sugar interactions. For the wD model, the oscillations are also considerably damped for the internucleotide base–sugar proton NOE's. The H1′–H4′ oscillations remain, however. This could be due to the sugar ring protons possessing a different effective correlation time but is more likely due to the fact that the wD sugar pucker does not exactly describe d(AC)$_4$·d(GT)$_4$. Using the sugar puckers in Table III for d(AC)$_4$·d(GT)$_4$ to calculate the H1′–H4′ NOE's results in a nearly complete smoothing out of the oscillations (see supplementary material).

## CONCLUSIONS

Semiquantitative analysis of DQF-COSY and 2D NOE spectra of d(AC)$_4$·d(GT)$_4$ clearly indicates a wrinkled structure for this oligomer in solution. If it is reasonable to give this time-averaged structure a single definition, we may say that it most closely approximates wD-DNA. We see that even half the number of methyl groups as are found in d(AT)$_n$ segments seems to promote wrinkling.

This study demonstrates that it is appropriate and desirable to apply more than one NMR structural technique to the study

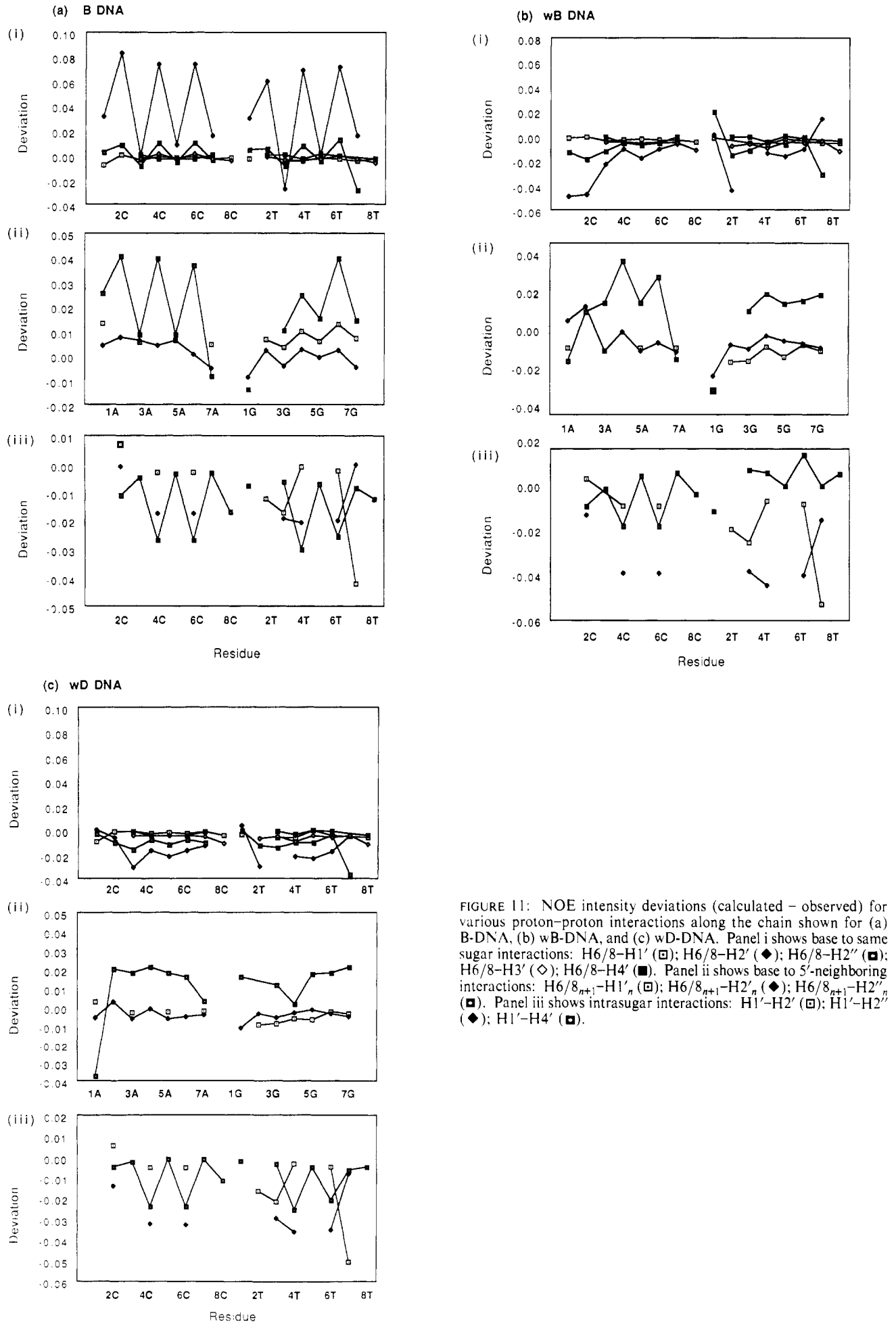


FIGURE 11: NOE intensity deviations (calculated − observed) for various proton–proton interactions along the chain shown for (a) B-DNA, (b) wB-DNA, and (c) wD-DNA. Panel i shows base to same sugar interactions: H6/8–H1′ (⊡); H6/8–H2′ (◆); H6/8–H2″ (■); H6/8–H3′ (◇); H6/8–H4′ (■). Panel ii shows base to 5′-neighboring interactions: H6/8$_{n+1}$–H1′$_n$ (⊡); H6/8$_{n+1}$–H2′$_n$ (◆); H6/8$_{n+1}$–H2″$_n$ (■). Panel iii shows intrasugar interactions: H1′–H2′ (⊡); H1′–H2″ (◆); H1′–H4′ (■).

of DNA oligomers. The DQF-COSY and 2D NOE data are independent but agree convincingly, lending confidence of the structural interpretations made. They give rise to separate structural constraints. They also show that both NMR experiments lead only to the definition of an average structure and give little or no information on the components of this average.

In the following paper, we describe a molecular dynamics study on $d(AC)_4 \cdot d(GT)_4$. From such a study, we may hope to obtain some picture of the dynamic nature of the time-averaged structure. In addition, we can define the time-averaged structure more exactly.

## ACKNOWLEDGMENTS

We gratefully acknowledge the use of the University of California, San Francisco, Computer Graphics Laboratory (supported by NIH Grant RR 01081). We thank Drs. U. Schmitz and S. Farr-Jones for helpful discussions and comments on the manuscript.

## SUPPLEMENTARY MATERIAL AVAILABLE

Figures A–C showing simulated deoxyribose 2′1′ and 2″1′ cross-peaks as a function of line width, simulations of the 1′2′, 2′1′, and 2″1′ cross-peaks for a series of values of $J_{1'2'}$ and $J_{2'3'}$, and a comparison of the error between calculated and experimental H1′–H4′ NOE's for three model structures of $d(AC)_4 \cdot d(GT)_4$, B-DNA, wD-DNA, and B-DNA, with sugar puckers altered to the values in Table III (4 pages). Ordering information is given on any current masthead page.

## REFERENCES

Altona, C., & Sundaralingham, M. (1972) *J. Am. Chem. Soc. 94*, 8205.

Arnott, S., Chandrasekaran, R., Puigjaner, L. C., Walker, J. K., Hall, I. H., & Birdsall, D. L. (1983) *Nucleic Acids Res. 11*, 1457.

Banks, K. M., Hare, D. R., & Reid, B. R. (1989) *Biochemistry 28*, 6996.

Boelens, R., Koning, T. M. G., & Kaptein, R. (1988) *J. Mol. Struct. 173*, 299.

Boelens, R., Koning, T. M. G., van der Marel, G. A., van Boom, J. H., & Kaptein, R. (1989) *J. Magn. Reson. 82*, 290.

Borgias, B. A., & James, T. L. (1988) *J. Magn. Reson. 79*, 493.

Borgias, B. A., & James, T. L. (1990) *J. Magn. Reson. 87*, 475.

Borgias, B. A., Thomas, P. D., & James, T. L. (1987, 1989) Complete Relaxation Matrix Analysis (CORMA), University of California, San Francisco.

Broido, M. S., Zon, G., & James, T. L. (1984) *Biochem. Biophys. Res. Commun. 119*, 663.

Broido, M. S., James, T. L., Zon, G., & Keepers, J. W. (1985) *Eur. J. Biochem. 150*, 117.

Celda, B., Widmer, H., Leupin, W., Chazin, W. J., Denny, W. A., & Wüthrich, K. (1989) *Biochemistry 28*, 1462.

Chary, K. V. R., Hosur, R. V., & Govil, G. (1987) *Biochemistry 26*, 1315.

Cheung, D. M., Kan, L.-S., Frechet, D., Ts'o, P. O. P., Uesugi, S., Shida, T., & Ikehara, M. (1984) *Biopolymers 23*, 775.

Denk, W., Baumann, R., & Wagner, G. (1986) *J. Magn. Reson. 67*, 386.

Drobny, G., Pines, A, Sinton, S., Weitekamp, D. P., & Wemmer, D. (1979) *Faraday Symp. Chem. Soc. 13*, 49.

Griesinger, C., Sørensen, O. W., & Ernst, R. R. (1985) *J. Am. Chem. Soc. 107*, 6394.

Havel, T. F., Kuntz, I. D., & Crippen, G. M. (1983) *Bull. Math. Biol. 45*, 665.

Hore, P. J. (1983) *J. Magn. Reson. 55*, 283.

Jarvis, L., Huang, C., Ferrin, T., & Langridge, R. (1986) Molecular Interactive Display And Simulation (MIDAS), University of California, Computer Graphics Laboratory, San Francisco.

Keepers, J. W., & James, T. L. (1984) *J. Magn. Reson. 57*, 404.

Lu, P., Cheung, S., & Donlan, M. (1985) *Adv. Biophys. 20*, 153.

Marion, D., & Wüthrich, K. (1983) *Biochem. Biophys. Res. Commun. 113*, 967.

Marion, D., & Bax, A. (1988) *J. Magn. Reson. 80*, 528.

Nilges, M., Clore, G. M., & Gronenborn, A. M. (1987) *Biochemistry 26*, 3718.

Olejniczak, E. T., Gampe, R. T., Jr., & Fesik, S. W. (1989) *J. Magn. Reson. 81*, 178.

Rinkel, L. J., & Altona, C. (1987) *J. Biomol. Struct. Dyn. 4*, 621.

Rinkel, L. J., van der Marel, G. A., van Boom, J. H., & Altona, C. (1987) *Eur. J. Biochem. 166*, 87.

Scheek, R. M., Boelens, R., Russo, N., van Boom, J. H., & Kaptein, R. (1984) *Biochemistry 23*, 1371.

Schmitz, U., Zon, G., & James, T. L. (1990) *Biochemistry 29*, 2357.

Singh, U. C., Weiner, P. K., Caldwell, J., & Kollman, P. A. (1986) AMBER 3.0: A Molecular Mechanics and Dynamics Program, University of California, San Francisco; Seibel, G. L. (1989) A Revision of AMBER, Revision A.

States, D. J., Haberkorn, R. A., & Ruben, D. J. (1982) *J. Magn. Reson. 48*, 286.

Suzuki, E., Pattabiraman, N., Zon, G., & James, T. L. (1986) *Biochemistry 25*, 6854.

van de Ven, F. J. M., & Hilbers, C. W. (1988) *Eur. J. Biochem. 178*, 1.

Weiss, G. H., & Ferretti, J. A. (1983) *J. Magn. Reson. 55*, 397.

Wemmer, D. E., Chou, S.-H., & Reid, B. R. (1984) *J. Mol. Biol. 180*, 41.

Widmer, H., & Wüthrich, K. (1986) *J. Magn. Reson. 70*, 270.

Wüthrich, K. (1986) *NMR of Proteins and Nucleic Acids*, Wiley, Interscience, New York.

Zhou, N., Bianucci, A. M., Pattabiraman, N., & James, T. L. (1987) *Biochemistry 26*, 7905.

Zhou, N., Manogaran, S., Zon, G., & James, T. L. (1988) *Biochemistry 27*, 6013.